Impact of forging direction on the recrystallization behaviour of nickel base superalloy AD730 billet material at subsolvus temperatures

Marcos Perez[1,*], Christian Dumont[2], Olivier Nodin[2], Sebastien Nouveau[2]

1. Advanced Forming Research Centre, University of Strathclyde, 85 Inchinnan Drive, Inchinnan, Renfrew (UK), PA4 9LJ.

2. Aubert & Duval, Site des Ancizes, BP1, 63770 les Ancizes Cedex, France

Abstract

AD730^{TM} is a newly developed Ni-based superalloy for turbine disk applications produced by cast and wrought processes. Conventional ingot-to-billet conversion is an expensive and very complex operation. Because of the difficulties to achieve a uniform strain for recrystallization, large unrecrystallized grains are retained along this process. Heterogeneities of grain size have a negative impact on subsequent forming processes as well as mechanical behaviour and ultrasonic inspectability of the destination part. The main aim of this work is to analyse the impact of both forging direction (billet, cogging) and strain (ε = 0.3 - 2) on the microstructural evolution of AD730 at subsolvus temperatures from a semi-finished product (billet) under conditions representative of both cogging and hot forging operations. Special attention to the presence of large unrecrystallized grains was paid. Double truncated cones (DTCs) were hot forged at subsolvus temperatures followed by air cooling. SEM and EBSD analysis were conducted in the as-received (billet) and the as-forged conditions. AD730 alloy presents a complex microstructure characterized by the presence of large unrecrystallized grains, aligned in the billet direction, with remarkable differences in γ' precipitates distribution as compared to recrystallized structures. The fine distribution of primary γ' precipitates (pinning effect) plays a key role on grain size control but also on the recrystallization behaviour. Continuous dynamic recrystallization (CDRX) mechanism was found to be operating in the large unrecrystallized grains, promoting the formation intragranular DRX grains and the gradual recrystallization of these grains. Strain presents a strong effect on the microstructural evolution of AD730, increasing the recrystallization fraction and refining the structure. By contrast, no significant effect associated to the forging direction was found. Conditions representative of cogging operations ($\varepsilon \leq 0.6$) at subsolvus temperatures were translated into large fractions of unrecrystallized structures (strain accumulation).

Keywords

AD730 alloy, hot forging, cogging, continuous dynamic recrystallization, γ' precipitates, EBSD analysis

1. Introduction

Nickel superalloys are used to manufacture high temperature rotary engine parts such as high pressure disks in gas turbine engines. In this application high strength at high operating temperatures is required due to the levels of stress and heat the disk must withstand. Additionally, the higher the temperature of a gas turbine engine the more fuel efficient it is, which is desirable for commercial airplane companies (1). Therefore, in order to stay competitive, it is necessary parts made from materials that can maintain mechanical strength at high temperatures whilst remaining comparatively low in cost. High strength turbine disks can be made from Nickel superalloys such as René 88DT, N18, RR1000, etc. However these alloys are manufactured by powder metallurgy which is an expensive and undesirable production route that can detract from the improved properties of the part (2). A manufacturing process referred to as the triple melt process has made the production of cast and wrought (C&W) nickel superalloys possible. This means that the balance of cost and performance at high temperature may be optimized.

AD730^{TM} is a newly developed Ni-based superalloy for turbine disk applications, with reported superior service properties around 700 °C when compared to Inconel 718 and several other alloys (2). This alloy is a γ′ strengthened alloy (≈ 40% γ′ volume fraction) produced by cast and wrought processes (3). The cast ingot is converted into billet during either cogging process or open die forging. The semi-finished billet is then further processed into its final geometry by forging, heat treating, and machining. Conventional ingot-to-billet conversion is an expensive and complex operation, requiring a significant amount of steps to break up the coarse as-cast structure and interdendritic regions. Due to the size of conventional ingots, it is difficult to achieve a uniformly high level of strain for recrystallization, resulting into non-recrystallized regions that retain large unrecrystallized grains. Grain size is one of the primary parameters controlling properties in these materials. The non-recrystallized regions will typically either fail the microstructural requirements for the final product or, if not detected, will lead to accelerated mechanical failure of the product. Non-uniform grain distributions will also affect the ultrasonic inspectability response, which is used to find flaws such as cracks, porosity, and large inclusions in billet, but also defects in the final component. The ultrasonic wave travel is affected by the microstructure. Non-uniform grain distributions, textured grain morphologies, and large unrecrystallized grains have a detrimental effect on the wave propagation and may mask defects, increasing the noise and leading to the rejection of the final and very expensive component.

Despite of the relevance of cogging process to the manufacturers of gas turbines, very little work has been already published for AD730 alloy in particular. In a recent work, the effect of three strain levels (ε = 0.5, 0.9 and 3) on the recrystallization behaviour of AD730 during hot forging at subsolvus temperatures was studied (4). The authors also found the presence of large unrecrystallized grains, regardless the strain level, in good agreement with the results reported in this work. From this work, the presence of intragranular precipitates in the interior of the large unrecrystallized grains can be inferred. However, the authors did not mention this characteristic feature and the interaction between recrystallization and γ' precipitates was not analysed. In the present work, intragranular precipitates were found to play a key role on strain distribution and subsequent recrystallization behaviour of the large unrecrystallized grains.

Concerning similar nickel base superalloys with high fraction of γ' precipitates, such as Udimet 720 and Waspaloy, limited work has been published reporting the mechanisms of microstructure evolution during ingot-to-billet conversion. In this sense, Y. Yu et al. (5) studied the deformation and recrystallization behaviour of a coarse-grain Udimet 720 ingot material at both supersolvus and subsolvus temperatures. Similarly, Semiatin et al. (6) studied the hot deformation and dynamic recrystallization behaviour of Waspaloy-ingot material with coarse columnar grains at supersolvus temperatures. Lindsley et al. (7) studied sub-solvus recrystallization behaviour in as-cast-wrought Udimet720Li with large grain sizes. Despite the similarities with AD730, these materials present significant differences in terms of forging and γ' solvus temperatures, fraction of primary γ' precipitates, etc. Therefore, a more deeply analysis of hot deformation behaviour and microstructure evolution of this novel nickel-base superalloys (AD730) during ingot-to-billet conversion is needed.

The main aim of this work is to analyse the effect of both forging direction and level of deformation on the microstructural evolution of the nickel base superalloy AD730 from a semi-finished product (billet) during hot forging at subsolvus temperatures (< 1100 °C). Conditions representative of deformation processes, such as cogging and hot forging operations, characterized by low and high levels of deformation, respectively, were selected. Double truncated cones (DTCs) were machined from a semi-finished billet, along both the billet and the cogging directions, covering a large range of strain [0.3 - 2 mm/mm]. Special attention was paid to both the recrystallization mechanisms which operate by promoting the recrystallization of large unrecrystallized grains and the interaction with γ' precipitates.

2. Material and experimental procedures

AD730 blocks from a 203mm diameter billet were supplied by Aubert & Duval (Les Ancizes, France). The chemical composition (wt. %) was 4% Fe, 8.5% Co, 15.7% Cr, 3.2 % Mo, 2.7% W, 2.25% Al, 3.4% Ti, 1.1% Nb, 0.01% B, 0.015% C and 0.03% Zr. Double truncated cones (DTCs) of ∅120 × 90 mm were machined along both the billet (BD) and the cogging directions (CD), see Figure 1. The hot forging trials of DTCs were carried out in hydraulic press at subsolvus temperatures (1070 °C), at a constant strain rate (0.05 s^{-1}) and with die temperatures of 435 °C. A 60% height reduction was introduced in one single blow. Prior to hot forging, the DTCs were preheated by isothermal holding during 1 hour at 1070 °C. After forging, the DTCs were cooled in air. Figure 2 shows the AD730 DTC forged in the billet direction, not showing either cracks or surface defects.

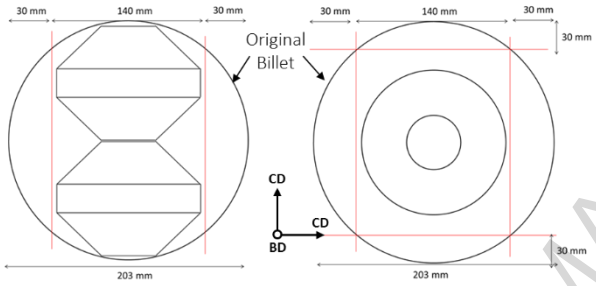

Figure 1. Schematic representation of the machining strategy of DTCs from ∅203 mm billet

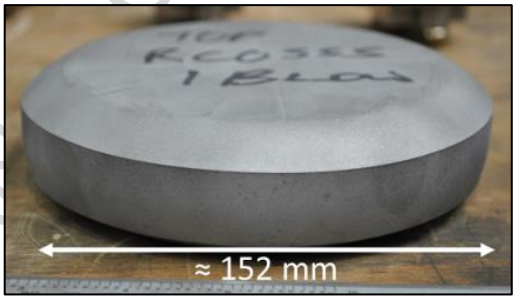

Figure 2. AD730 DTC hot forged at subsolvus temperature

For the metallurgical analysis, sections of DTCs were cut by Electron Discharging Machining (EDM). The surface for metallurgical analysis were prepared by conventional grinding and polishing techniques. Both Scanning Electron Microscopy (SEM) and Electron Backscatter Diffraction technique (EBSD) were used. FEM simulations were run in DEFORM software for the forging temperature of 1070 °C. Figure 3 shows the strain distribution across a DTC section forged at 1070 °C in one single blow with a 60% of height reduction. Microstructural analysis of the hot forged DTCs were conducted at 8 positions along the central section, covering a large range of strains [0.3 – 2 mm/mm]. Table 1 shows the strain distribution for the 8 selected regions.

EBSD scans were performed by using TSL Electron Backscatter Diffraction (EBSD) attached to a FEI Quanta 650 scanning electron microscope (FEI) operating at 20kV. EBSD maps were collected from the processed samples using a step size of 0.5 μm. Index ratios above 95% were obtained in all the cases. Channel 5 software provided by HKL Technology was used for data analysis. Standard clean-up procedure (grain dilation) was applied before analysing the obtained EBSD data. In this study, EBSD images are mainly represented by band contrast (BC), local misorientation (LM) and inverse pole figures (IPF) by using Channel 5 - Tango software. BC is an electro backscatter

diffraction pattern (EBSP) quality parameter that indicated the sharpness of Kirkuchi bands, where deformed regions and grain boundaries are associated to low BC values. LM component displays the average misorientation among consecutive data points, discarding misorientations over a certain value associated to subgrain or grain boundaries. In the present study a filter size of 3 × 3 and a maximum misorientation angle of 5˚ was considered. IPF maps show the crystallographic direction of the orientation in colour codes. In some cases, BC, LM and IPF figures are combined with grain boundaries maps (GB), where red, black, and blue lines correspond, in most of the cases, to low angle (LAGB, 2˚< θ <15˚), high angle (HAGB, θ >15˚) and annealing twin boundaries (Σ3, <111> 60˚), respectively. For grain size measurements, 15˚ misorientation angle was considered, excluding twin boundaries (Σ3, <111> 60˚).

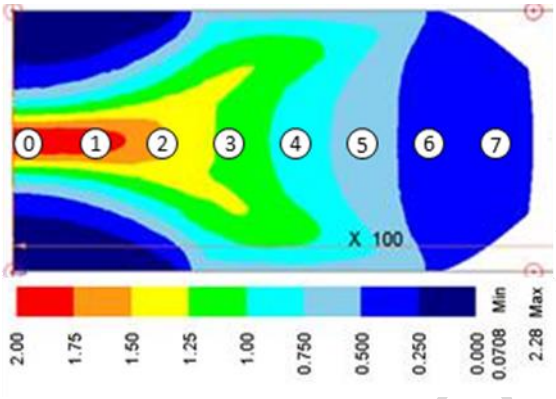

Figure 3. FEM simulation of effective strain distribution of hot forged AD730 DTCs

Position	Effective strain
0	≈ 2.0
1	≈ 1.8
2	≈ 1.5
3	≈ 1.2
4	≈ 0.9
5	≈ 0.6
6	≈ 0.4
7	≈ 0.3

Table 1. Strain distribution for the 8 selected regions of hot forged AD730 DTCs

In order to investigate in more detail microstructural aspects such as nucleation mechanisms, misorientation profiles in the interior of deformed grains, enlarged regions at higher magnifications from EBSD maps were analysed and discussed in the present work. The separation of DRX grains from deformed matrix (partitioned DRX grains) for detailed analysis of recrystallized grains was conducted by using the recrystallization fraction component, available in Channel 5 software. A grain misorientation and internal average misorientation angle (ϑ_c) of 15˚ and 2˚ were used, respectively. For the analysis of the hot deformation structure of deformed grains at the three forging temperatures, misorientation distributions by using point-to-point (local) and point-to-origin (cumulative) misorientations across grains were used. The Brandon's criterion was employed to identify and analyse coincident site lattice (CSL) boundaries (8). It can be expressed as follows:

$$v_m = 15 \cdot \Sigma^{-1/2}, \qquad \textit{Equation 1}$$

where v_m is the maximum angular deviation which can be accommodated in an Σ boundary.

In order to understand the interaction of γ' precipitates with recrystallization at subsolvus temperatures, a sample from the as-received condition were heat treated during 1 hour at 1070 °C, simulating the soaking treatment of DTCs prior to forging, followed by water quenching. The main aim was to avoid any potential precipitation during cooling to room temperature. The γ' precipitates distribution was revealed by etching with Agua Regia. A direct comparison between the as-received and the as-preheated conditions was carried out.

3. Results and Discussion

3.1. Microstructure in the as-received condition

Microstructural analysis of AD730 alloy in the as-received condition (billet) was conducted. Figure 4 shows a combination of EBSD maps: IPF, BC + GB, LM. From these maps, it is clear that AD730 material is characterized by a complex and heterogeneous microstructure. Fully recrystallized grains (strain-free) with a large density of annealing twin boundaries (Σ3) in their interior were found. By contrast, large unrecrystallized grains, strongly aligned in the billet direction, with a large density of intragranular LAGB were observed. In the interior of the unrecrystallized grains, nucleation and growth of small recrystallized grains, also aligned along the billet direction, were found (see yellow arrow in Figure 4.b). Similar small recrystallized grains were detected in those regions located in between unrecrystallized grains (red arrow in Figure 4.b).

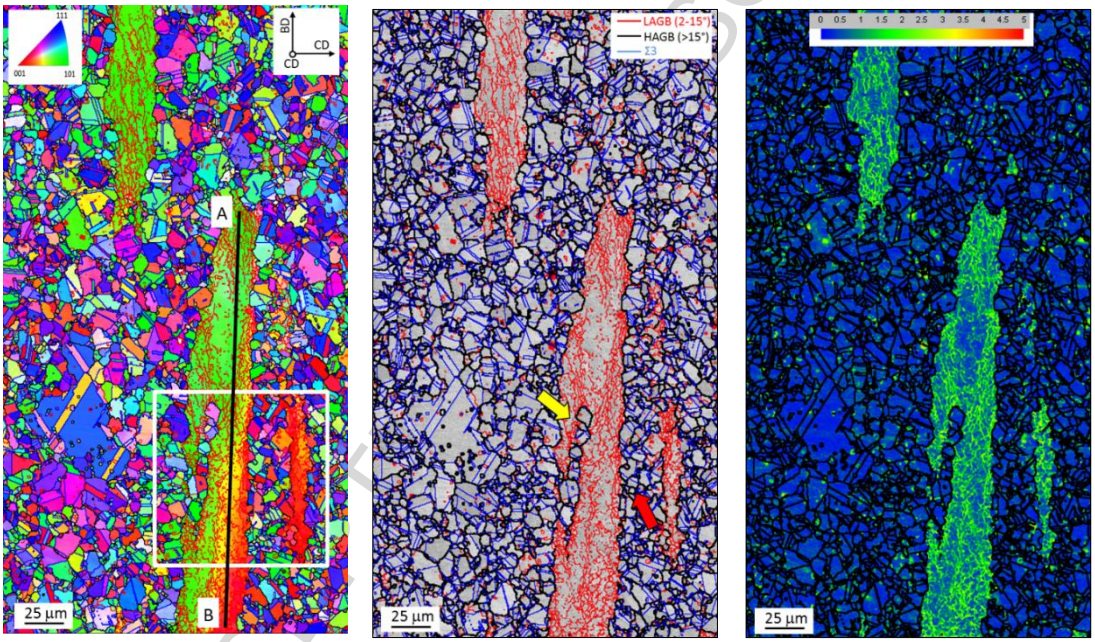

a) IPF map *b) BC + GB map* *c) LM map*

Figure 4. EBSD analysis of AD730 material in the as-received condition. Red, black and blue lines denote low (>2°, high angle (>15° and Σ3 boundaries, respectively.

Figure 5 shows the misorientation developed across a large unrecrystallized grain along both the cogging and billet directions. This unrecrystallized grain presents a remarkable cumulative misorientations, up to 35 °, in the billet (Figure 5.b), along the line AB (Figure 4.a), and cogging direction (line EF, Figure 5.d) as a result of the successive forging operations. Point-to-point misorientations, clearly exceeding 2˚, was observed, mainly in those regions close to the grain boundaries (line CD, Figure 5.c), denoting both internal subdivision associated to subgrain formation and inhomogeneous strain accumulation. Even the formation of high angle boundaries (>15°) in the interior of unrecrystallized grains can be detected (white arrows, Figure 5).

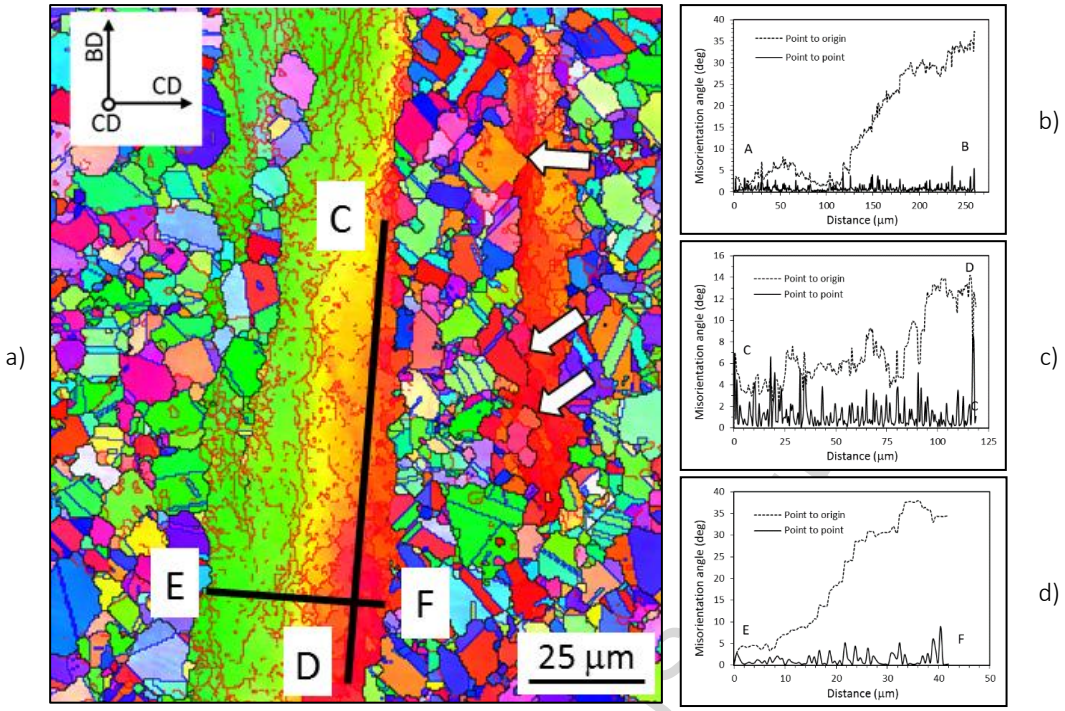

Figure 5. Detail of unrecrystallized grain (Zoom of Figure 4) and misorientation distribution for AD730 in as-received condition (billet)

In terms of γ' precipitates, large differences between recrystallized and unrecrystallized grains were found (Figure 6.a). In the fully recrystallized regions (Figure 6.b & d), characteristic primary and secondary γ' precipitates for this type of alloys with high fraction of γ' precipitates (> 40%) can be observed. By contrast, the unrecrystallized grains present a much finer distribution of small primary γ' precipitates (Figure 6.c & e).

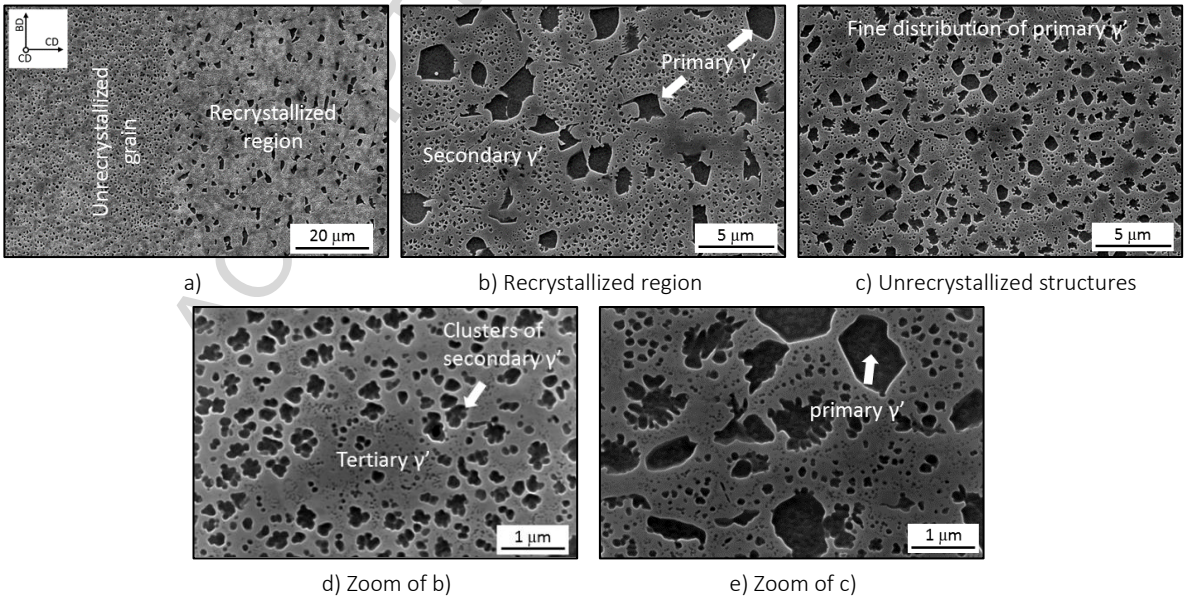

a) b) Recrystallized region c) Unrecrystallized structures

d) Zoom of b) e) Zoom of c)

Figure 6. Differences in primary γ' precipitates between recrystallized and unrecrystallized grains for AD730 in as-received condition (billet)

3.2. Microstructure in the as-preheated condition

In the as-preheated condition (1070 °C during 1h followed by water quenching), see Figure 7.a, a significant number of large unrecrystallized grains can be identified (yellow arrows). Differences in the size of primary γ' precipitates are still quite evident between unrecrystallized grains and recrystallized regions (Figure 7.b).

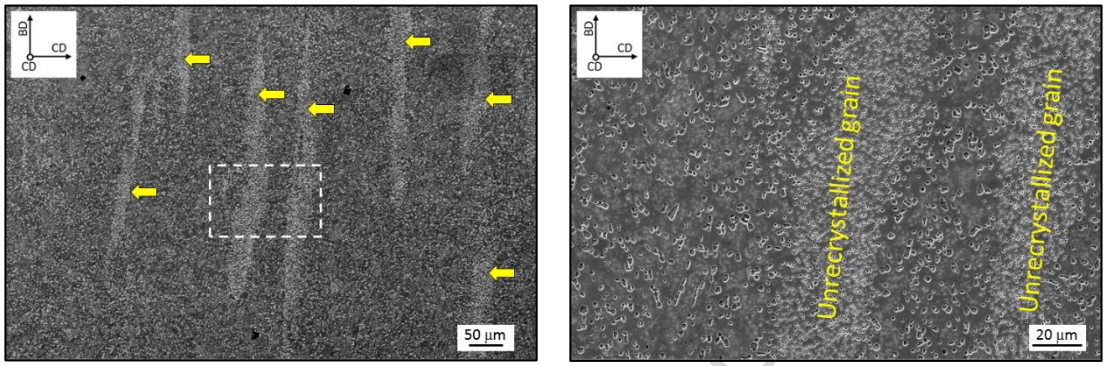

a) b) Zoom of a)

Figure 7. Differences in primary γ' precipitates between recrystallized and unrecrystallized grains for AD730 in as-preheated condition (billet)

Figure 8 show the impact of preheat treatment on the distribution of primary and secondary γ' precipitates in both recrystallized and unrecrystallized regions. In recrystallized regions, primary γ' precipitates seem not to be affected by soaking treatments at subsolvus temperature, although coalescence of primary γ' precipitates was found (Figure 8.d), in agreement with the results reported by F. Masoumi *et al*. (9). A large density of secondary γ' precipitates remain undissolved after 1 hour of soaking time at 1070 °C (Figure 8.e). Globulization of the largest secondary particles and dissolution of the smaller ones is observed. Within the unrecrystallized grains, dissolution of the smallest secondary γ' precipitates were detected, but the fine distribution of primary γ' precipitates is retained prior to hot forging (Figure 8.f).

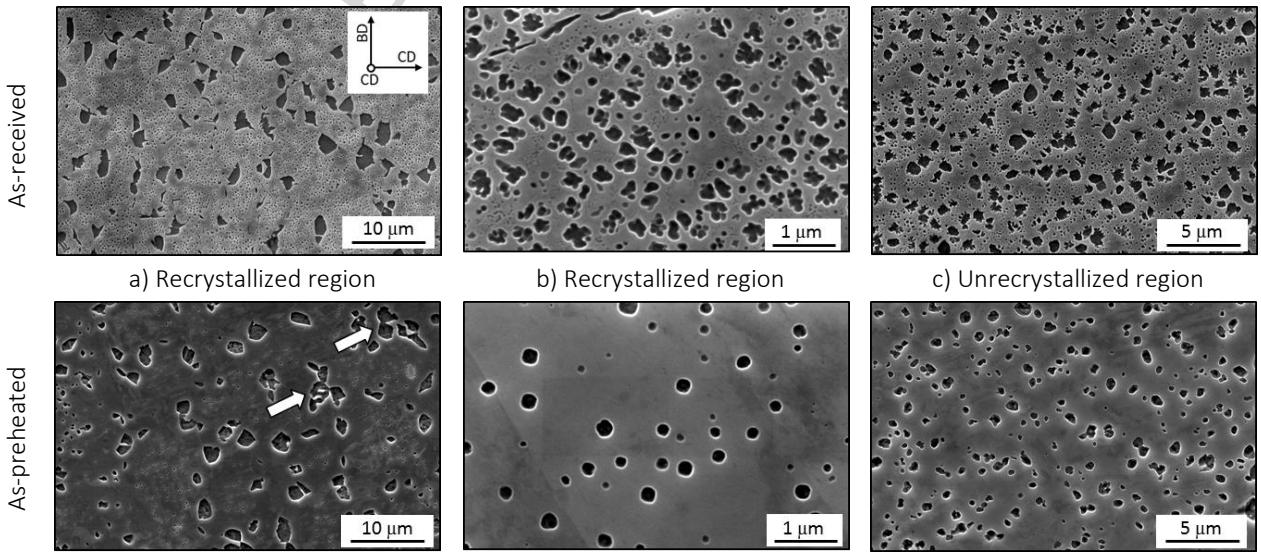

a) Recrystallized region b) Recrystallized region c) Unrecrystallized region

d) Recrystallized region e) Recrystallized region f) Unrecrystallized region

Figure 8. Effect of preheating treatment on the distribution of primary and secondary γ' precipitates for both recrystallized and unrecrystallized regions of AD730 alloy.

3.3. Microstructure in the as-forged condition

Microstructural analysis by EBSD was carried out in the as-forged condition in order to investigate mainly the evolution of large unrecrystallized grains as a function of both strain and forging direction. Figure 9 depicts IPF maps from the forged DTCs at three positions 1, 4 & 6 which correspond to regions with high (ε ≈ 1.8), medium (ε ≈ 0.9) and low levels (ε ≈ 0.4) of deformation, respectively, from DTCs forged in the billet and cogging directions. The forging direction of the DTCs corresponds to the vertical direction in all the cases.

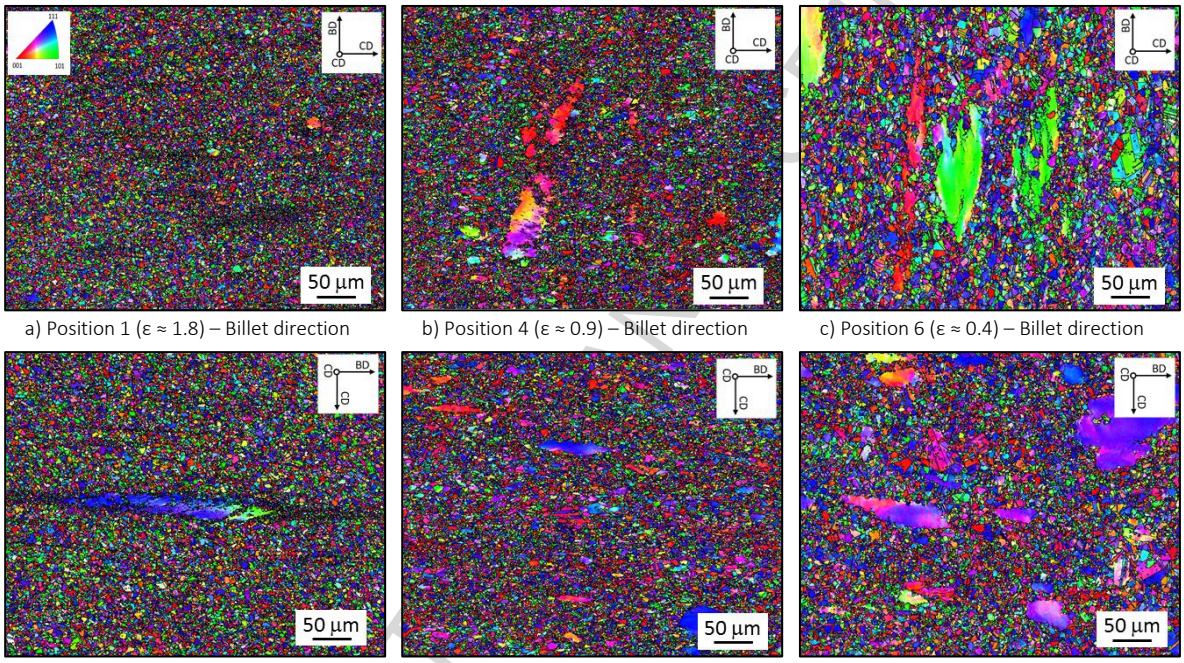

a) Position 1 (ε ≈ 1.8) – Billet direction
b) Position 4 (ε ≈ 0.9) – Billet direction
c) Position 6 (ε ≈ 0.4) – Billet direction
d) Position 1 (ε ≈ 1.8) – Cogging direction
e) Position 4 (ε ≈ 0.9) – Cogging direction
f) Position 6 (ε ≈ 0.4) – Cogging direction

Figure 9. EBSD analysis (IPF) at different positions of AD730 DTCs forged in the billet and cogging directions. (1070 °C, 60% height reduction in one single blow). Black lines denote high angle boundaries (>15°).

In the Position 1, with a high level of deformation (ε ≈ 1.8), dark elongated areas aligned along the compression plane are observed, regardless the forging direction, see Figure 9.a & d. In this sense, an enlarged area from Figure 9.d is shown in Figure 10.a & b. These figures depict what seems to be a "*tail*" of the large unrecrystallized grain, partially recrystallized, which is formed by a fine distribution of small equiaxed grains. These results clearly indicate that these dark regions are, in fact, regions with high density of HAGB associated to prior large unrecrystallized grains as confirmed by Figure 10.c. This latter figure shows the presence of fine γ' precipitates in a region with small equiaxed grains, similar in size as those observed in the large unrecrystallized grains (Figure 8.c & f).

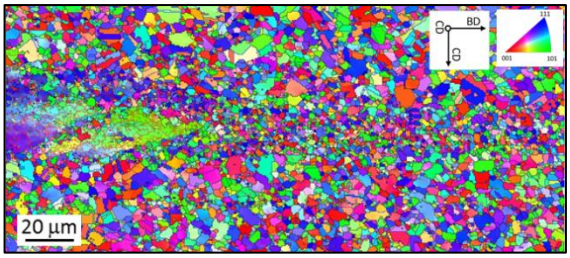

a) IPF map

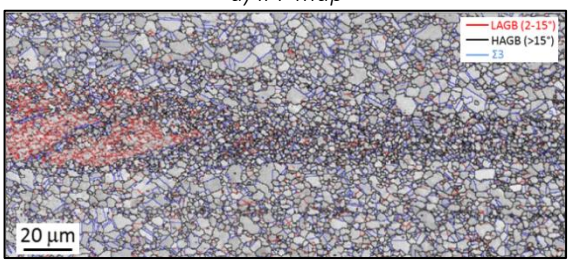

b) BC + GB map

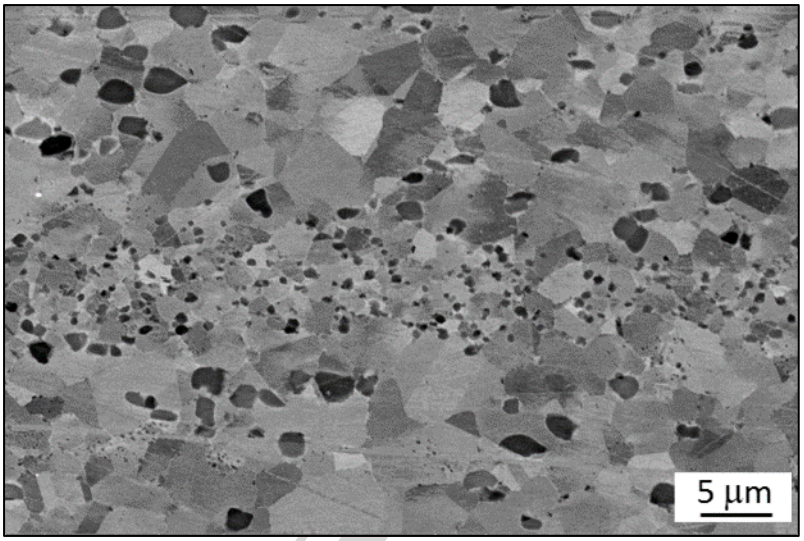

c) Backscatter SEM image

Figure 10. Position 1 (ε ≈ 1.8) – DTC forged in the cogging direction (CD)

Another interesting aspect observed in those regions subjected to significant levels of deformation is the presence of a large density of Σ3 boundaries in the interior of large unrecrystallized grains. Figure 11 and Figure 12 show two clear examples which correspond to position 2 (ε ≈ 1.5) and position 1 (ε ≈ 1.8) from the DTCs forged in the billet (BD) and cogging (CD) directions, respectively. Misorientation profiles are plotted in Figure 11.c & d and Figure 12.c for both positions, respectively. From point-to point misorientations, it is noticeable is the presence of a large amount of Σ3 boundaries (<111> 60°), but also intragranular misorientations which clearly exceed 10˚. From point-to-origin profiles, alternating lattice orientations were observed for the DTC forged in BD, see Figure 11.c & d. This type of misorientation development generally is associated with the formation of sets of parallel microbands (10) as confirmed by the IPF map (Figure 11.b). A total cumulative misorientation of about 50˚ and 40˚ was found along the lines A-B (billet direction, Figure 11.c) and C-D (cogging direction Figure 11.d), respectively. For DTC forged in the BD (Figure 12), the deformation patterns is different. This grain has developed a long range continuous orientation gradients, see line C-D of Figure 12.c, denoted by the gradual accumulation of misorientations across the grain, up to 30˚.

In those regions with lower strain distributions (Figure 9.b-f), Positions 4 (ε ≈ 0.9) and 6 (ε ≈ 0.4), increasing fractions of unrecrystallized grains were found. The unrecrystallized grains were partially divided/broken into smaller grains. With the exception of the orientation of the large unrecrystallized grains, no apparent differences associated to the forging direction were found.

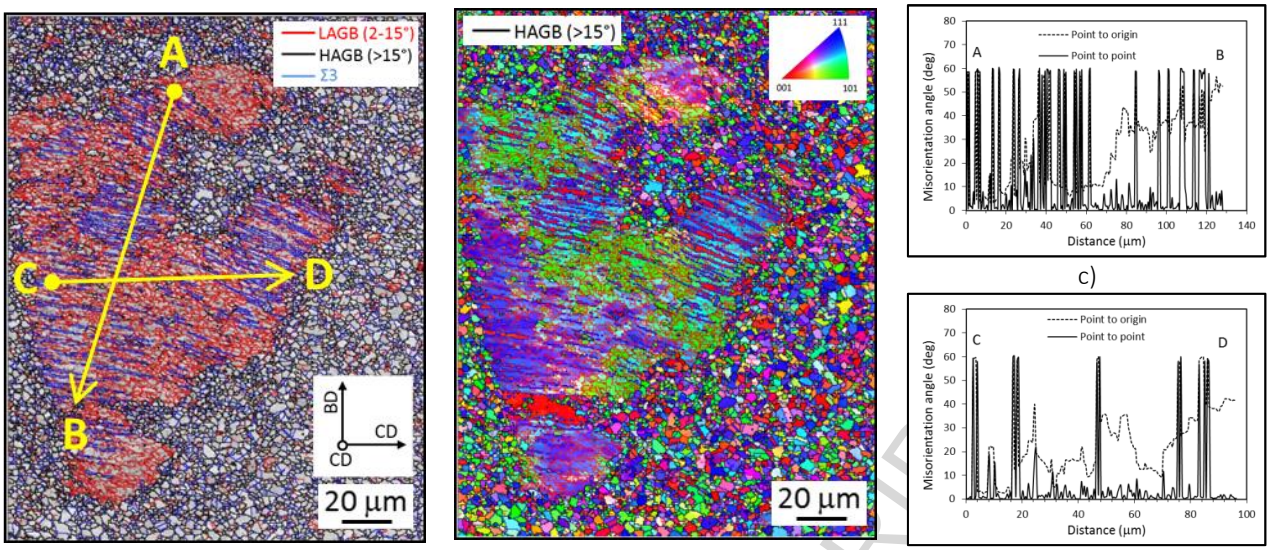

Figure 11. Position 2 (ε ≈ 1.5) – DTC forged I the billet direction (BD)

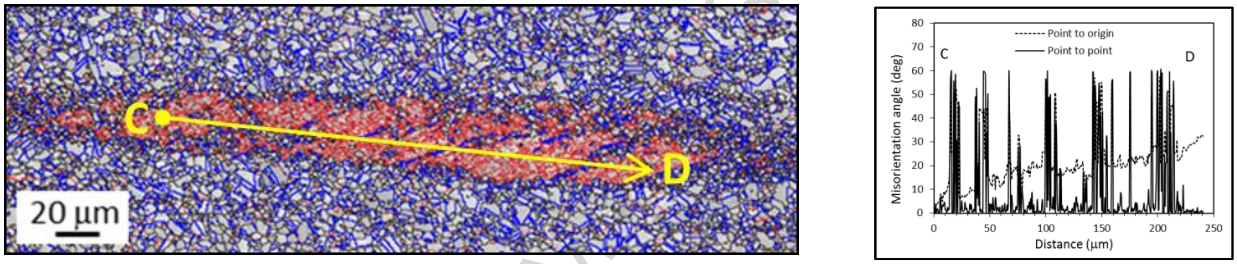

Figure 12. Position 1 (ε ≈ 1.8) – DTC forged I the cogging direction (CD)

Concerning those regions subjected to low levels of deformation (**ε** ≤ 0.6), a high proportion of unrecrystallized grains with the characteristic large density of internal LAGB were observed. In addition, coarse grains with internal twin boundaries were also observed in these regions, see white/black dotted squares in Figure 13.

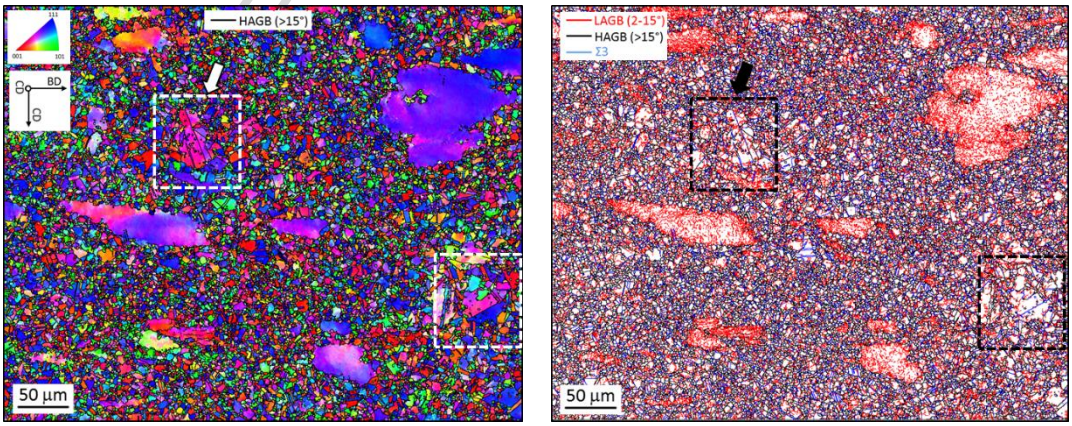

a) Inverse Pole Figure map (IPF) *b) Grain Boundary map (GB)*

Figure 13. Position 6 (ε ≈ 1.4) from AD730 DTC forged in the cogging direction (CD)

Figure 14.a-c shows a more detailed analysis of a coarse grain structure from the enlarged region shown in Figure 13 (the one marked by white/black arrows). A combination of IPF, LM and BC + GB maps was used. Variations of

local crystallographic orientations in the interior of the coarse grain are observed in the IPF figure (Figure 14.a). From the BC + GB maps (Figure 14.b) a relatively high density of intragranular LAGBs and the presence of disrupted twin boundaries, partially transformed into regular HAGB (white arrows), was found. The local misorientation map (Figure 14.c) confirms the significant strain accumulated within this grain. In the as-received condition (Figure 14.d-e), similar coarse structures were found but free of deformation.

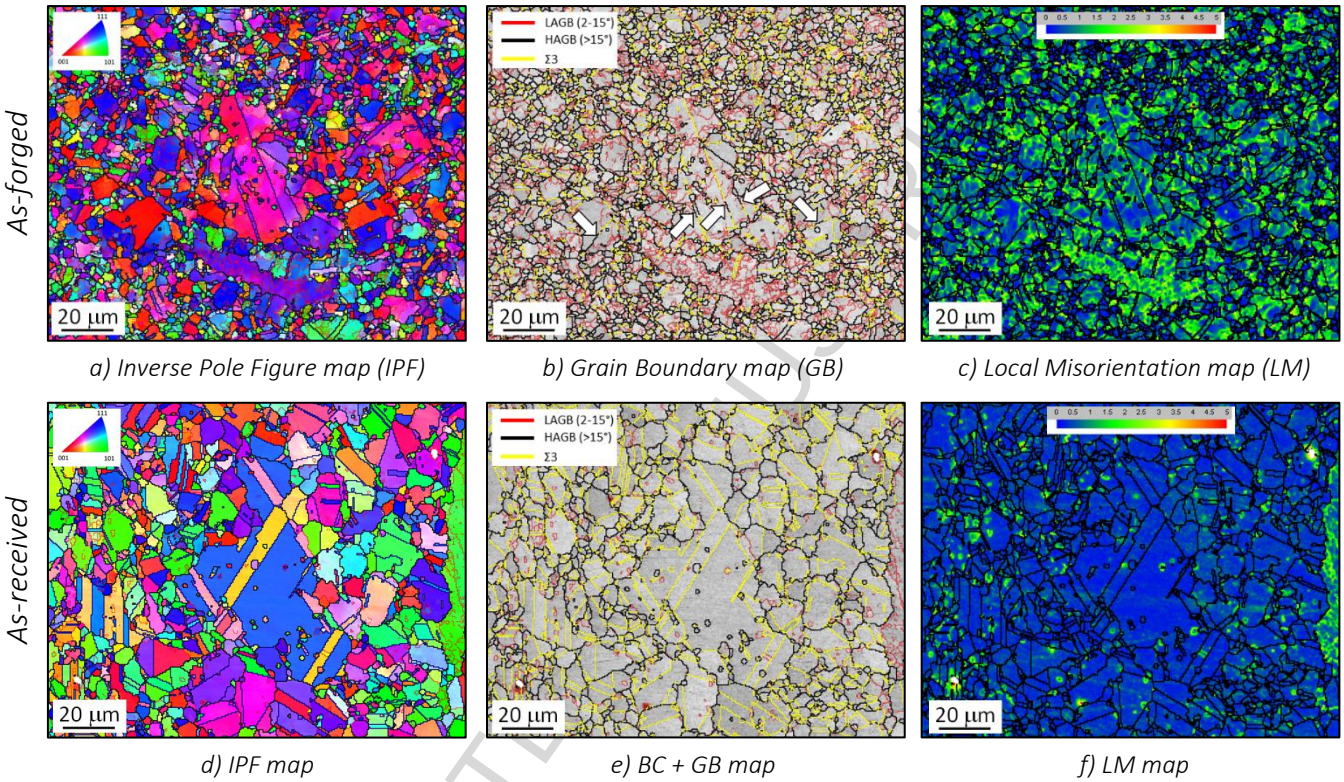

a) Inverse Pole Figure map (IPF) *b) Grain Boundary map (GB)* *c) Local Misorientation map (LM)*

d) IPF map *e) BC + GB map* *f) LM map*

*Figure 14. Detail of coarse grain structures in as forged condition (Position 6, **ε ≈ 0.4,** DTC forged in the cogging direction (a,b,c) and in the as-received condition (d,e,f)*

Figure 15 depicts an example of an unrecrystallized grain located in a region with the lowest strain (position 7, ε ≈ 0.3) from the DTC forged in the billet direction (BD). From Figure 15.a & b, It is evident not only the large fraction of LAGB in the interior of this grain, but also the presence of HAGB aligned in the original billet direction, splitting/dividing this grain. It is clear that the formation of internal HAGB provides nucleation sites for the formation and growth of intragranular grains. Although these intragranular grains resemble new DRX grains, based on the different crystallographic orientation with respect the parent grain (Figure 15.a) and the presence of internal twin boundaries (Figure 15.b), the local misorientation map (Figure 15.c) clearly reveals the significant amount of deformation (misorientation) within these intragranular grains.

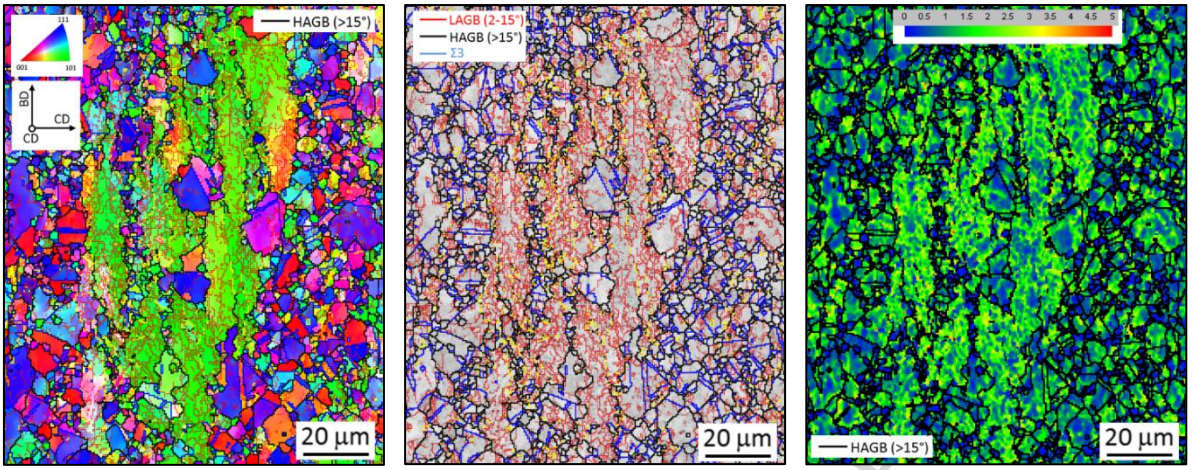

a) IPF map b) BC + GB map c) LM map

*Figure 15. Detail of unrecrystallized grain from Position 7 (**ε ≈ 0.3**) of DTC forged in the billet direction (BD)*

In order to shed more light about the impact of forging direction and strain on the microstructure of AD730 alloy, Figure 16 plots the recrystallized fraction component for the 8 analysed positions of both DTCs forged in the billet and cogging directions, respectively. Due to the size of the EBSD maps, only 50% of the scanned area is included in this latter figure. Figure 17 plots the results from the recrystallization fraction component (Figure 16) as a function of the strain. A linear relationship of the recrystallized fraction with the strain was found. The fraction of strain-free structures increases from 20-30% for the lowest level of deformation (ε ≈ 0.3) up to 80% in those positions with maximum deformation (ε ≈ 2). Forging direction does not present any significant effect. Similar results/tendencies were observed for both DTCs forged in the billet (BD) and cogging direction (CD).

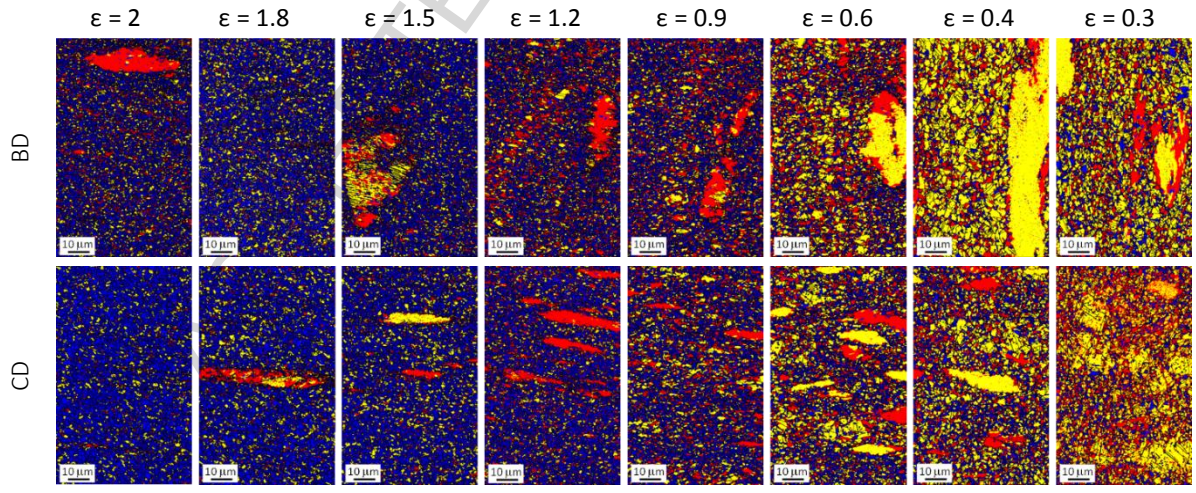

*Figure 16. Recrystallization fraction component of AD730 DTCs forged in the billet (BD) and cogging directions (CD) as function of the strain (**ε** = 0.3 – 2 mm/mm). Blue, yellow and red colours correspond to recrystallized, structured and deformed grains, respectively.*

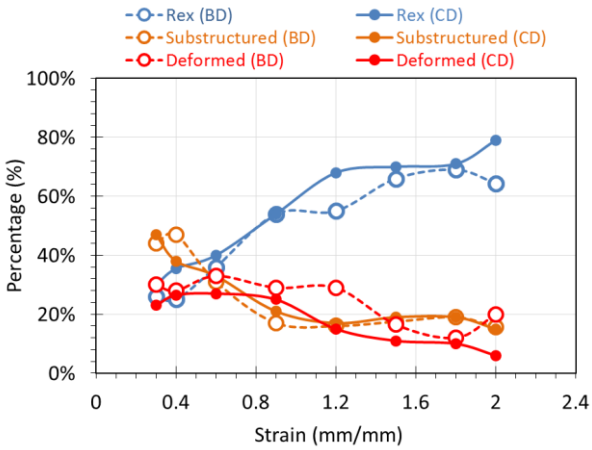

Figure 17. Fractions of recrystallized, substructure and deformed grains (recrystallized fraction component) versus the effective strain for AD730 DTCs forged in the billet (BD) and cogging (CD) directions.,

Figure 18 plots the evolution of misorientation distribution, in terms LAGB ($2^{\circ} < \theta < 10^{\circ}$), MAGB ($10^{\circ} < \theta < 15^{\circ}$), HAGB ($\theta > 15^{\circ}$), and special boundaries (Σ3, Σ9 & Σ27), with the effective strain for both DTCs forged in the billet (BD) and cogging (CD) directions. Recrystallized (Rex) and unrecrystallized structures (UnRex) have been analysed separately. In recrystallized regions, see Figure 18.a, a linear increase of HAGB is accompanied by a reduction of LAGB as strain increases, in good agreement with the larger recrystallized fractions in regions with higher amount of deformation (Figure 17). A similar tendency is observed for Σ3, Σ9 & Σ27 boundaries (Figure 18.b). It is clear that strain level presents a strong effect on the microstructural evolution of AD730 during hot forging at subsolvus temperatures (1070 °C). Concerning the impact of forging direction, similar values and tendencies were observed in the DTC hot forged in the cogging (CD) and billet direction (BD).

On the other hand, the separate analysis of unrecrystallized regions, Figure 18.c & d, reveals that the presence of large fractions of LAGB (>80%) as a results of the intragranular misorientations developed in the interior of deformed grains. From these figures, no significant differences associated to either forging direction (CD, BD) or strain level were found. For a strain of 1.5 mm/mm (DTC forged in BD) a significant drop in LAGB is accompanied by an increase in HAGB, see Figure 18.c. This peculiar behaviour is associated to the presence of Σ3 boundaries in the interior of a large unrecrystallized grain, see Figure 11, as confirmed by Figure 18.d. In this latter figure, the evolution of Σ9 & Σ27 were not plotted as the fraction of these boundaries is 0.0 % in most of the cases, with maximum values below 0.03% in a very few positions.

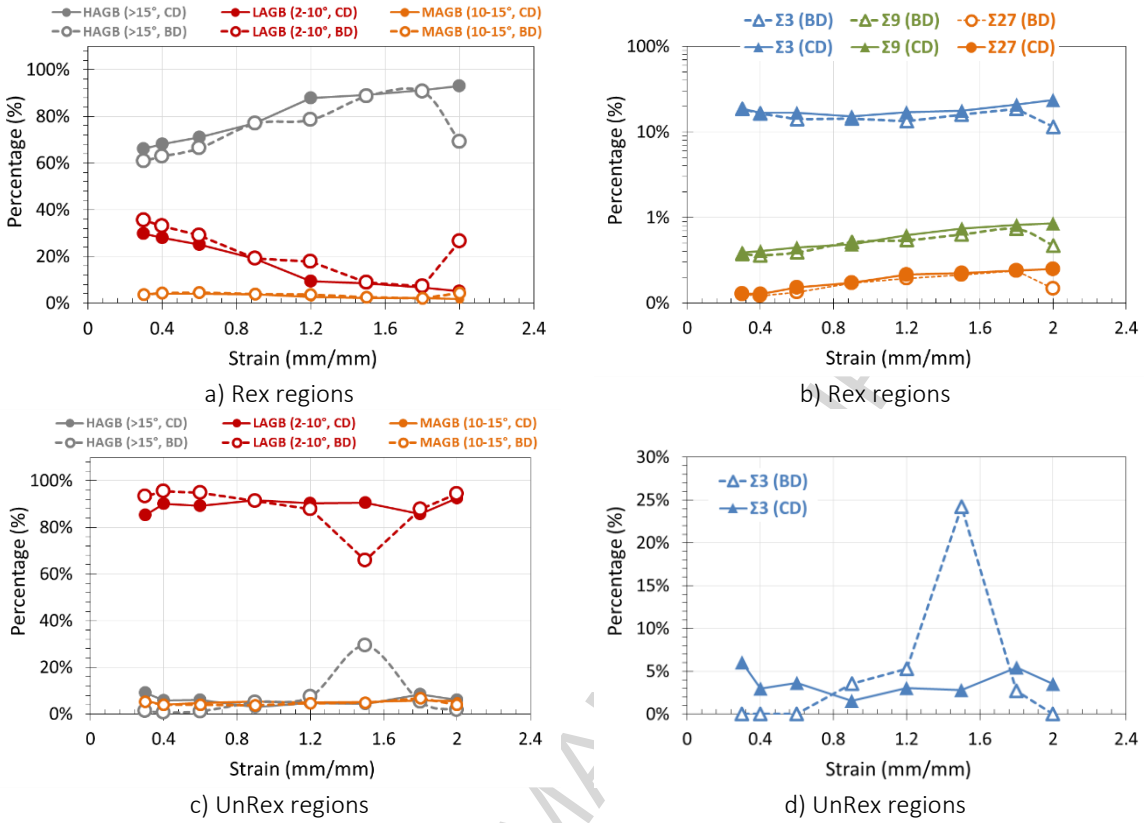

Figure 18. Evolution of LAGB (2˚< ϑ <10˚), MAGB (10˚< ϑ <15˚), HAGB (ϑ >15˚), CSL and Σ3, Σ9 and Σ27 boundaries with effective strain for AD730 DTCs forged in the billet (BD) and cogging (CD) directions for recrystallized (Rex) and unrecrystallized (UnRex) regions,

The mean grain size for both recrystallized (Rex) and unrecrystallized (UnRex) structures versus the effective strain is plotted in Figure 19.a. Unrecrystallized regions presents larger mean grain sizes in those positions with lower levels of deformation ($\varepsilon \leq 0.6$ mm/mm). In recrystallized regions, the mean grain size is less dependent on strain than in the unrecrystallized regions. Note that the mean grain size in unrecrystallized regions decreases sharply with strain. Concerning the impact of forging direction (BD, CD) no significant differences were found across recrystallized and unrecrystallized regions.

Concerning the maximum grain size (largest unrecrystallized grain), see Figure 19.b, the DTC forged in the cogging direction presents a slightly but consistent smaller grain sizes than that forged in billet direction.

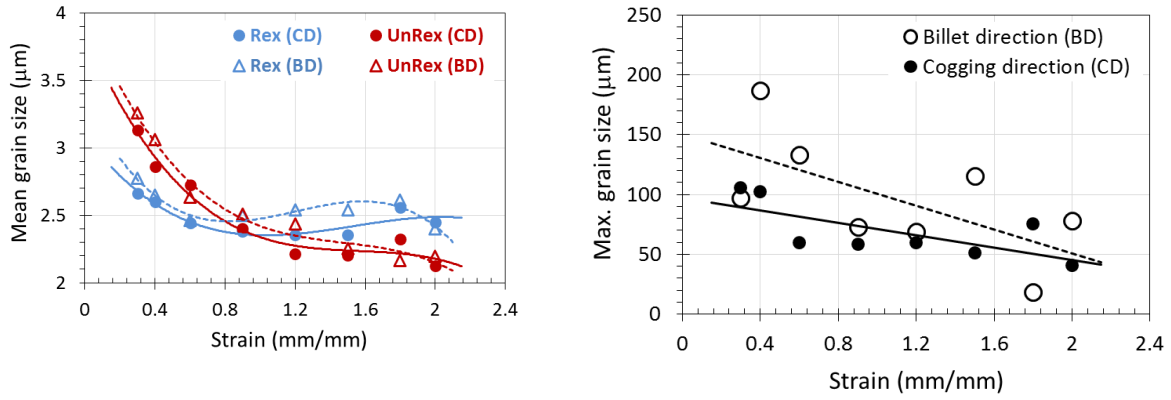

a) b)

Figure 19. Evolution of mean grain size in recrystallized (Rex) and unrecrystallized (UnRex) regions a) and maximum grain size b) with effective strain for AD730 DTCs forged in the billet (BD) and cogging (CD) directions.

Figure 20.a plots the fractions of the coherent twin boundaries (CT Σ3) which satisfy the Brandon criterion ($v/v_m \leq 0.2$) for both DTCs. Initially, the fraction of CT Σ3 boundaries increases linearly with the strain from up to ε = 0.9-1.2 for BD and CD, respectively, remaining constant or increasing slightly in those positions with the highest level of deformation (ε ≥ 0.8 - 1.2). Again, no significant differences associated to the forging direction were found. Linear relationships between the recrystallized fraction and CT Σ3 boundaries ($v/v_m \leq 0.2$) were found, see Figure 21, with regression coefficients R^2= 0.94 and 0.97 for the DTCs forged in the billet and cogging directions, respectively. These results clearly confirm the strong dependency between both variables, indicating that most of the CT Σ3 are within the recrystallized grains (strain-free), turning into incoherent twin boundaries (ICT) as a result of deformation.

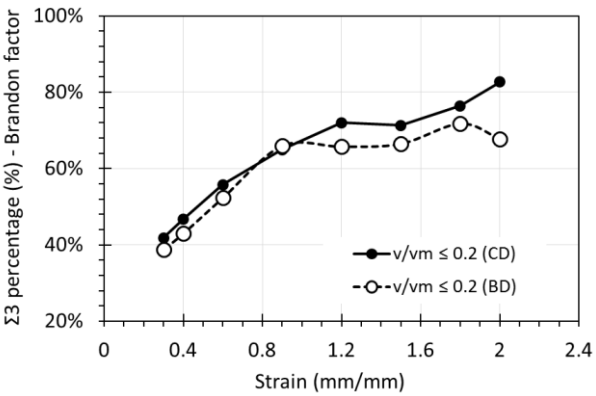

Figure 20. Fraction evolution of Σ3 boundaries which satisfy the Brandon criterion ($v/v_m \leq 0.2$) with effective strain for AD730 DTCs forged in the billet (BD) and cogging (CD) directions.,

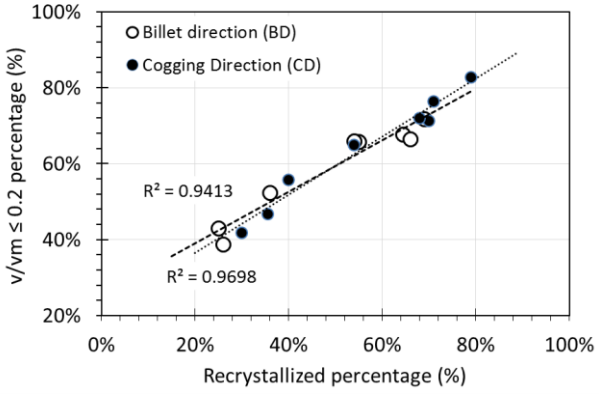

Figure 21. Relationship between the fraction of Σ3 which satisfy the Brandon criteria ($v/v_m \leq 0.2$) and percentage of fully recrystallized (strain-free) grains for AD730 DTCs forged in the billet (BD) and cogging (CD) directions.

4. Discussion

Structural constituents

AD730 alloy presents a complex microstructure with a mixture of several constituents with significant differences in size, dislocation density and substructure. Three main types of constituents were found for AD730:

- Small equiaxed grains which correspond to fully recrystallized (strain-free) grains. The large fraction and its small size provided a remarkable grain refinement and high levels of recrystallization in those regions subjected to significant amount of deformation ($\varepsilon \geq 1.2$). It is well known that grain size depends strongly in aspects such as grain boundary mobility, and then on forging temperature (11). This is the case for nickel base superalloys with low fraction of γ' precipitates, such as Nimonic 80a, conventionally forged well above the solvus temperatures (12). However, for nickel base superalloys such as AD730, forged at subsolvus temperatures, the pinning effect of γ' precipitates plays a key role on grain size control, but also acting as main barriers to GB motion for the occurrence of DRX (5). A direct relationship between interparticle spacing of primary γ' precipitates and grain size is expected (5). This latter one is confirmed by Figure 10.c showing a region fully recrystallized characterized by the presence small equiaxed grains and a fine distribution of γ' precipitates in grain boundaries and triple points. These observations confirm the strong pinning effect of the γ' precipitates and provide an explanation to the remarkable small grain size distributions observed in the "*dark areas*" (see Figure 9.a & d). These results also indicates that the fine distribution of γ' precipitates, associated to prior unrecrystallized grains (Figure 8.c & f), is retained despite both the enhanced grain boundary diffusion of HAGB and deformation enhanced diffusion (5), even in regions with a remarkable amount of deformation (position 1, $\varepsilon \approx 2$). It seems that the drop in temperature after hot forging (air cooling) did not provide enough time for the occurrence of mechanisms such as the coarsening/dissolution of the fine γ' precipitates, reducing the pinning force and therefore allowing the small recrystallized grains to growth and to develop an homogeneous grain structure.

- In regions of the DTCs with low levels of deformation, coarse grain structures characterized by their equiaxed morphology, internal variations of crystallographic orientations and disrupted twin boundaries were detected, see Figure 13 and Figure 14.d-e. The original straight coherent twin boundaries, characterized by 60° rotation around the <111> axis, were gradually converted to general high-angle

boundaries with straining, and losing their original Σ3 coincidence site lattice orientation relationship (13), (14). Very similar coarse structures were also observed in the as-received condition, but free of deformation as shown in Figure 14.d-e. ~~In contrast with DTCs which were cooled in air after hot forging, the forged billet (supplied condition) go through furnace cooling to avoid potential cracking during cooling. Either slow cooling after hot forging or prior soaking treatments could provide enough time for the occurrence of static recrystallization and grain growth processes. These mechanisms could explain the main microstructural differences found between the as-received (billet) and the as-forged condition from DTCs. Mechanisms such as abnormal grain growth processes associated to low levels of deformation during the hot forging trials of the DTCs should be dismissed.~~

- Large unrecrystallized grains, strongly aligned originally along the original billet direction, present a substructure characterized by a large density of LAGB with misorientation well above 2°. These grains develop large misorientation gradients with the formation of medium to high angle boundaries in their interior, especially close to the grain boundaries, denoting inhomogeneous strain distribution. It is well accepted that there are generally more slip systems operating near grain boundaries than in the interior of grains (15). These results indicate that the fragmentation original grains occurred in the course of heterogeneous deformation, leading to the accumulation of misorientation gradients and the potential local formation of HAGBs and therefore nucleation sites for DRX grains (5). Boundaries with high misorientations were also observed in the grain interior associated to the development of geometrically necessary ~~dislocation~~ boundaries (GNBs) or deformation bands (16).

In contrast with discontinuous dynamic recrystallization (DDRX) characterized by the nucleation of new DRX grains by grain boundary bulging following by growth (17),the formation of arrays of low angle boundaries and a gradual increase in the boundary misorientations through accumulation and rearrangement of the dislocations during deformation (18) (19). For AD730, the strong pinning effect of the fine distribution of γ' precipitates inhibit/halt the growth of DRX grains at the expense of the large unrecrystallized grains. This latter one results into strain accumulation during the successive cogging operations, and promotes therefore the occurrence of continuous dynamic recrystallization (CDRX) mechanism, as confirmed by the formation of intragranular MAGB, even HAGB, required for the nucleation of DRX (20). For AD730, different stages of the hot deformation and recrystallization behaviour of the large unrecrystallized grains by means of CDRX mechanism were observed:

1. Subgrains formation by means of the generation of subboundaries (LAGB ≥ 2°);
2. Increase of subgrains misorientation resulting into the formation of MAGB (10-15°);
3. Separation/isolation of new grains from parent grain through formation of HAGB (deformation bands).

With the accumulated strain, microstructure fragmentation accelerated the occurrence of deformation bands, providing nucleation sites for the nucleation and growth of new recrystallized grains in the interior of unrecrystallized grains (intragranular DRX) in AD730 at sub-solvus deformation temperature. Figure 15 confirms that the occurrence of grain fragmentation with the formation of deformation bands, playing a critical role on the (gradual) consumption of the large unrecrystallized grains and therefore on the microstructural evolution of AD730. These results are in agreement with those reported for Udimet 720 (5) and Waspaloy (21) alloys, also with the absence of obvious classical necklace microstructure.

Impact of strain and forging direction

In the present work, variables such as the misorientation distribution (LAGB, MAGB, HAGB, Σ3, Σ9 & Σ27) see Figure 18), mean and maximum grains size (μm, Figure 19), recrystallization fraction (%, Figure 17), fraction of coherent twin boundaries (CT Σ3, see Figure 20) were quantified and plotted versus the effective strain (ε = 0.3 - 2 mm/mm). From these results, it is clear that strain presents the strongest effect on the microstructural evolution of AD730 alloy during hot forging at subsolvus temperatures (1070 °C). A linear increase in the fraction of fully recrystallized structures (strain-free grains), from 20-30% up to 80%, as effective strain increases was found. The increase in recrystallized structures is accompanied by growing fractions of HAGBs, Σ3, Σ9 & Σ27 boundaries, and reduction of the mean & maximum grain size (large unrecrystallized grains) and LAGBs.

Strains, as high as 1.5-2 mm/mm, are required to develop structures with high levels of recrystallization (80%). However, the presence of a large unrecrystallized grain in Figure 16 demonstrates that strains as high as 2 mm/mm do not warranty the attainment of a fully new-grained structure (100%). The combination of relative small levels of strain (ε ≤ 0.6). at subsolvus temperatures is translated into large fractions of unrecrystallized structures (above 40%), see Figure 17. A significant level of deformation can be inferred not only in the interior of the large unrecrystallized grains, see Figure 13.b, but also on small and coarse grains, see Figure 14.c and Figure 15.c. As commented previously, the analysis of coarse structures from regions of DTC with low levels of deformation confirms the significant strain accumulated within this sort of coarse structures in the as-forged condition. Similar conclusions come up with the analysis of intragranular DRX grains presenting a significant

deformation in their interior (Figure 15), indicating that the nucleation and growth of these grains took place prior to the hot forging of the DTCs. These results could indicate that the cogging process characterized by open die forging operations with low levels of deformation ($\varepsilon \leq 0.6$) at subsolvus temperatures is translated into large fractions of unrecrystallized structures (strain accumulation). However, the differences between the as-received (billet) and as-forged conditions (DTCs) suggest that aspects such ~~cooling rate or furnace/~~soaking treatment could play a very important role on the microstructural evolution of AD730 alloy. In the present work, the DTCs were preheated during 1 hour prior to hot forging. The results from Figure 8.e clearly indicates that the selected soaking time was insufficient to dissolve the secondary γ' precipitates in the interior of the recrystallized structures (matrix). The presence of a fine distribution of secondary γ' precipitates could provide a strong interactions with migrating grain boundaries (DRX), especially in those regions with low levels of deformation ($\varepsilon \leq 0.6$) where the driving force for recrystallization is lower.

Concerning the forging direction (billet *vs*. direction), the evolution of recrystallization fraction with strain follows a similar tendency for both DTCs forged in the billet and cogging directions. No significant differences in the distribution of LAGB, MAGB, HAGB, Σ3, Σ9 and Σ27 boundaries were found in recrystallized and unrecrystallized regions. These results are in contrast to the evident morphological and structural differences found in the large unrecrystallized grains across both forging directions. In the as-received condition (Figure 4, Figure 5), the large unrecrystallized grains are originally strongly aligned in the billet direction showing an elongated morphology (low aspect ratio) as a result of the successive deformation steps during the cogging process. These grains develop a long range continuous orientation gradients associated to the gradual accumulation of misorientations (see Figure 5). Similar deformation patterns were observed in the DTC forged in the cogging direction as shown in Figure 12.b. The deformation in the billet direction is forcing the large unrecrystallized grains to change their macroscopic shape, adopting a more globular morphology (high aspect ratio) and therefore reducing the surface area. These macroscopic changes impose strong deformation redistributions promoting the development of deformation bands with alternating lattice orientations, as shown in the *point-to-origin* misorientation profiles in Figure 11.c-d. With increasing levels of deformation, these deformation bands increase the misorientation between neighbour bands, developing intragranular HAGB and eventually splitting large unrecrystallized grains into smaller grains.

Despite the macroscopic shape change and the aforementioned substructural changes, no significant benefits in terms of recrystallized fraction (see Figure 17) associated to forging in the billet direction were found. Even, consistent larger unrecrystallized grains were found in the DTC forged in the billet direction than in the cogging direction, see Figure 19.b. The reduction in surface area as the large unrecrystallized grains adopt a more globular morphology could reduce the overall contribution of CDRX mechanism. Note that the formation of complex substructures with the formation of MAGB and HAGB was observed in those regions close to the grain boundaries as a result of heterogeneous deformation.

Evolution of CSL (Coincidence site lattice) boundaries

CSL boundaries are characterized by the specific misorientation values and the reciprocal density of coinciding sites as defined as Σ. Primary twins Σ3 are characterized by 60˚ misorientation around <111>. Twins can be formed during deformation (mechanical twinning) or recrystallization. New annealing twin boundaries may form due to interaction of pre-existing Σ3 boundaries during grain boundary migration or growth accidents at the migrating grain boundaries (22) (23). The propagation of glissile dislocations across grain boundaries can produce addition {111} steps, increasing the probabilities of twin generation (24). The high proportion of annealing twin boundaries (Σ3) in the interior of the recrystallized grains clearly demonstrate the important role of twinning on the recrystallization behaviour of AD730 alloy.

A large density of Σ3 boundaries in the interior of large unrecrystallized grains were observed in those regions subjected to significant levels of deformation ($\varepsilon \geq 1.5$), as shown in Figure 11 and Figure 12. Twinning is an important deformation mechanism of the superalloys at intermediate temperature where ductility is low (25). However, at temperatures as high as 1070 °C, clear evidences that twinning at the interface is operating at early stages of the recrystallization process for AD730 alloy were found. These results are good agreement with those reported by H. Zhang et al. (26) who studied the effect of deformation parameters on the twinning evolution of nickel base superalloy during hot deformation. The authors found that during hot deformation, the original Σ3 boundaries lost their Σ3 misorientation due to crystal rotations, while lots of new Σ3 boundaries were formed mainly by growth accident. In the present work, the transformation of the migrating HAGBs, formed by means of CDRX mechanism, into Σ3 boundaries by growth accidents can explain the observed results.

Twin Σ3 boundaries can be classified as coherent (CTs) and incoherent Σ3 boundaries (ICT). Coherent twins are immobile, presenting a very low interface energy due to the perfect arrangement of grain boundary atoms. This type of boundaries are characterized by a straight and parallel morphology (23). Incoherent Σ3 boundaries are, by contrast, very mobile. It is broadly accepted that the relative deviation (v/v_m) provides an estimation of plane type and boundary energy (23) (27) (28), where v and v_m are the deviation from the ideal twin orientation and the maximum allowable deviation angle, respectively. It is accepted that the upper deviation limit of coherent Σ3 boundaries is 0.2 (28). Linear relationships, with regression coefficients (R^2) well above 0.9, were found between strain-free grains (recrystallized structures) and the fraction of Σ3 boundaries which satisfy the Brandon criteria ($v/v_m \leq 0.2$), see Figure 21. This signifies that the large fractions of Σ3 boundaries in the interior of new DRX grains (strain-free) are CT boundaries, in agreement with the appearance of the twins with a straight and parallel morphology. As deformation proceeds, Σ3 boundaries rotate from the ideal orientation (<111> 60°) becoming ICT Σ3 or even regular HAGB, as shown in Figure 14.b.

5. Conclusions

From the microstructural analysis evolution of AD730 billet material during hot forging at subsolvus temperatures, the following conclusions are made:

- A very fine distribution of intragranular (primary) γ′ precipitates within the large unrecrystallized grains were found. These precipitates play an important role on the DRX mechanisms which operate on AD730, promoting the occurrence of CDRX. Subgrain rotation, by increasing the misorientation from LAGB to MAGB and HAGB, dominates over the progress of hot deformation of AD730 alloy at subsolvus temperatures. Intragranular DRX nucleation associated to both close to grain boundaries and deformation bands, plays an important role on the gradual recrystallization of large unrecrystallized grains. Twinning at the interface (migrating boundary) operates at early stages of the recrystallization process of AD730 alloy.
- Strain presents the strongest effect on the microstructural evolution of AD730. Increasing fractions of recrystallization structures, HAGB, CSL, Σ3, Σ9 and Σ27 boundaries as strain increases were found:
    - Strains above $\varepsilon \geq 1.2$, characteristic of hot forging operations, promote the development of high fractions of recrystallized structures;
    - Strains below $\varepsilon \leq 0.6$, characteristic of cogging operations, result into large fraction of unrecrystallized structures and therefore into strain accumulation.
- No significant differences in the microstructural evolution associated to the forging direction were observed, despite the significant morphological and structural differences found in the large unrecrystallized grains. Forging in the billet direction is forcing the large unrecrystallized grains to change their macroscopic shape, adopting a more globular morphology which, in turn, could reduce the overall contribution of CDRX mechanism on the consumption of these grains.
- A large density of secondary γ′ precipitates remain undissolved after 1 hour of soaking time at 1070 °C for AD730. The fine distribution of undissolved precipitates, prior to hot forging, could provide a strong interaction with migrating grain boundaries (DRX), resulting into large fractions of unrecrystallized structures in those positions of DTCs with relative low level of deformation ($\varepsilon \leq 0.6$).

- ~~Structural differences between the as-received and the as-forged conditions indicate that either slow cooling rates after forging or furnace heat treatments prior to forging are playing a key role on the microstructural evolution of AD730~~.

6. Acknowledgements

The corresponding author would like to acknowledge Aubert & Duval for the help provided in terms of supplied material, advice and fruitful discussions. The corresponding author also wants to acknowledge the Advanced Forming Research Centre (AFRC) for its support in this project.

7. References

[1] R.C. Reed; The Superalloys, Fundamentals and Applications, Cambridge University Press, Cambridge, 2006.

[2] A. Devaux, B. Picqué, M.F. Gervais, E. Georges, T. Poulain, P. Héritier, AD730^{TM} - A New Nickel-Based superalloy for high temperature engine rotative parts, in: E.S. Huran, R.C. Reed, M.C. Hardy, M.J. Mills, R.E. Montero, P. D. Portella, J. Telesman (Eds.), Superalloys 2012: 12th International Symposium on Superalloys, TMS (The Minerals, Metals & Materials Society), 2012, pp. 911-919.

[3] A. Devaux, A. Helstroffer, J. Cormier, P. Villechaise, J. Douin, M. Hantcherli, F. Pettinari-Sturmel, Effect of aging heat-treatment on mechanical properties of AD730 superalloy, in: A. Banik, X. Liu, I. Dempster, K. Heck, J. Andersson, J. Groh, T. Gabb, R. Helmink, A. Wusatowska-Sarnek (Eds.), 8th International Symposium on Superalloys 718 and Derivatives, TMS (The Minerals, Metals & Materials Society), 2014, pp. 521-535.

[4] T. Konkova, S. Rahimi, S. Mironov, T.N. Baker, Effect of strain level on the evolution of microstructure in a recently developed AD730 nickel based superalloy during hot forging, Mater. Charact., 139 (2018), 437-445. https://doi.org/10.1016/j.matchar.2018.03.027

[5] Q.Y. Yu, Z.. Yao and J.X. Dong, Deformation and recrystallization behaviour of a coarse-grain, nickel-base superalloy Udimet720Li ingot material, Mater. Charact. 107 (2015) 398-410. https://doi.org/10.1016/j.matchar.2015.07.035.

[6] S.L. Semiatin, D.S. Weaver, R.C. Kramb, P.N. Fagin, M.G. Glavicic, R.L. Goetz, N.D. Frey, M.M. Antony, Deformation and recrystallization behavior during hot working of a coarse-grain, nickel-base superalloy Ingot material, Metall. Mater. Trans. A 35 (2004) 679-684. https://doi.org/10.1007/s11661-004-0379-y.

[7] B. Lindsley, X. Pierron, Sub-solvus recrystallization mechanisms in Udimet alloy 720Li, in: T.M. Pollock, R.D. Kissinger, R.R. Bowman (Eds.), Superalloys 2000, TMS (The Minerals, Metals & Materials Society), 2000, pp. 59–68.

[8] D.G. Brandon, The structure of high-angle grain boundaries, Acta Metall., 14 (1966) 1479-1484. https://doi.org/10.1016/0001-6160(66)90168-4.

[9] F. Masoumi, M. Jahazi, D. Shahriari, J. Cormier, Coarsening and dissolution of γ' precipitates during solution treatment of AD730™ Ni-based superalloy: Mechanisms and kinetics models, J. Alloys Compd. 658 (2016) 981-995. https://doi.org/10.1016/j.jallcom.2015.11.002.

[10] D. Jorge-Badiola, A. Iza-Mendia and I. Gutierrez, Evaluation of intragranular misorientation parameters measured by EBSD in a hot worked austenitic stainless steel, J. Microscopy, 228 (2007) 373-383. DOI: 10.1111/j.1365-2818.2007.01850.x.

[11] Y.C. Lin, X.Y. Wu, X.M. Chen, J. Chen, D.X. Wen, J.L. Zhang, L.T. Li, EBSD study of a hot deformed nickel-base superalloy, J. Alloys Compd. 640 (2015) 101-113. https://doi.org/10.1016/j.jallcom.2015.04.008.

[12] M. Pérez, Microstructural evolution of Nimonic 80a during hot forging under non-isothermal conditions of screw press, J. Mater. Process. Technol., 252 (2018), pp. 45-57. http://dx.doi.org/10.1016/j.jmatprotec.2017.09.014.

[13] J.P. Thomas, F. Montheillet and S.L. Semiatin. Modelling of Microstructure Evolution during Thermomechanical Processing of Nickel-Base Superalloys, in D.U. Furrer and S.L. Semiatin. ASM Handbook, Vol. 22a (Eds), Fundamentals of Modelling for Metals Processing, 2009, pp. 566-582.

[14] D. Jorge-Badiola, A. Iza-Mendia, I. Gutierrez, Study of EBSD of the development of the substructure in a hot deformed 304 stainless steel, Mater. Sci. Eng. A, 394 (2005) 445-454. doi: 10.1016/j.msea.2004.11.049

[15] F.J. Humphreys, M. Hatherly, Recrystallization and related annealing phenomena, second ed., Elsevier, Oxford, 2004.

[16] B.Bay, N.Hansen. D.A.Hughes, D.Kuhlmann-Wilsdorf, Overview no. 96 evolution of f.c.c. deformation structures in polyslip, Acta Metall. Mater. 40 (1992) 205-219. https://doi.org/10.1016/0956-7151(92)90296-Q.

[17] Z. Yanushkevich, A. Belyakov, R. Kaibyshev, Microstructural evolution of a 304-type austenitic stainless steel during rolling at temperatures of 773-1273 K. Acta Mater. 82 (2015) 244-254. https://doi.org/10.1016/j.actamat.2014.09.023.

[18] Y. Wang, W.Z. Shao, L. Zhen, X.M. Zhang, Microstructure evolution during dynamic recrystallization of hot deformed superalloy 718, Mater. Sci. Eng. A 486 (2008) 321-332. https://doi.org/10.1016/j.msea.2007.09.008.

[19] S. Gourdet, F. Montheillet, An experimental study of the recrystallization mechanism during hot deformation of aluminium, Mater. Sci. Eng. A 283 (2000) 274-288. https://doi.org/10.1016/S0921-5093(00)00733-4.

[20] D. Pongea, G. Gottstein, Necklace formation during dynamic recrystallization: mechanisms and impact on flow behavior, Acta Mater. 46 (1998) 69-80. https://doi.org/10.1016/S1359-6454(97)00233-4.

[21] G. Shen, S.L. Semiatin, R. Shivpuri, Modeling microstructural development during the forging of Waspaloy Metall. Mater. Trans. A 26 (1995) 1795-1803. https://doi.org/10.1007/BF02670767.

[22] S. Mandal, A.K. Bhaduri and V. Subramanya Sarma, Role of twinning on dynamic recrystallization and microstructure during moderate to high strain rate hot deformation of a Ti-modified austenitic stainless steel, Metall. Mater. Trans. A 43 (2012) 2056-2068. https://doi.org/10.1007/s11661-011-1012-5.

[23] S. Qin, H. Zhang, J. Liu, W. Zheng, Electron backstattered diffraction analysis of the effect of deformationn temperature on the microstructure evolution in a typical nickle-based superalloy durig hot deformation, J. Meter. Res. 31 (2016) 1348-1360. https://doi.org/10.1557/jmr.2016.159.

[24] Y. Cao, H. Di, J. Zhang, J. Zhang, T. Ma, R.D.K. Misra, An electron backscattered diffraction study on the dynamic recrystallization behaviour of a nickel-chromium alloy (H800) during hot deformation, Mater. Sci. Eng. A 585 (2013) 71-85. https://doi.org/10.1016/j.msea.2013.07.037

[25] I.S. Kim, B.G. Choi, H.U. Hong, Y.S. Yoo, C.Y. Jo, Anomalous deformation behavior and twin formation of Ni-base superalloys at the intermediate temperatures, Mater. Sci. Eng. A, 528 (2011), 7149-7155. https://doi.org/10.1016/j.msea.2011.05.083

[26] H. Zhang, H. Zhou, S. Qin, J. Liu, X. Xu, Effect of deformation parameters on twinning evolution during hot deformation in a typical nickel-base superalloys, Mater. Sci. Eng. A, 696 (2017), pp. 290-298. https://doi.org/10.1016/j.msea.2017.04.077

[27] V. Randle, P. Davies, Deviation from reference plances and reference misorientation for Σ3 boundaries, Interface Sci. 7 (1999) 5-13. https://doi.org/10.1023/A:1008734331685.

[28] M.L. Kronberg, F.H. Wilson, Secondary recrystallization in copper, Trans Met Soc AIME, 185 (1949), 501–514.

[29] S. Mandal, A.K. Bhaduri, V. Subramanya Sarma, Studies on twinning and grain boundary character distribution during anomalous grain growth in a Ti-modified austenitic stainless steel, Mater. Sci. Eng. A, 515 (2009) 134-140. https://doi.org/10.1016/j.msea.2009.02.042.

8. Data availability

The raw/processed data required to reproduce these findings cannot be shared at this time as the data also forms part of an ongoing study.

9. Figure captions

Figure 1. Schematic representation of the machining strategy of DTCs from ∅ 203 mm billet

Figure 2. AD730 DTC hot forged at subsolvus temperature

Figure 3. FEM simulation of effective strain distribution of hot forged AD730 DTCs

Figure 4. EBSD analysis of AD730 material in the as-received condition. Red, black and blue lines denote low (>2°, high angle (>15° and Σ3 boundaries, respectively.

Figure 5. Detail of unrecrystallized grain (Zoom of Figure 4) and misorientation distribution for AD730 in as-received condition (billet)

Figure 6. Differences in primary γ' precipitates between recrystallized and unrecrystallized grains for AD730 in as-received condition (billet)

Figure 7. Differences in primary γ' precipitates between recrystallized and unrecrystallized grains for AD730 in as-preheated condition (billet)

Figure 8. Effect of preheating treatment on the distribution of primary and secondary γ' precipitates for both recrystallized and unrecrystallized regions of AD730 alloy.

Figure 9. EBSD analysis (IPF) at different positions of AD730 DTCs forged in the billet and cogging directions. (1070 °C, 60% height reduction in one single blow). Black lines denote high angle boundaries (>15°).

Figure 10. Position 1 (ε ≈ 1.8) – DTC forged in the cogging direction (CD)

Figure 11. Position 2 (ε ≈ 1.5) – DTC forged I the billet direction (BD)

Figure 12. Position 1 (ε ≈ 1.8) – DTC forged I the cogging direction (CD)

Figure 13. Position 6 (ε ≈ 1.4) from AD730 DTC forged in the cogging direction (CD)

Figure 14. Detail of coarse grain structures in as forged condition (Position 6, ε ≈ 0.4, DTC forged in the cogging direction (a,b,c) and in the as-received condition (d,e,f)

Figure 15. Detail of unrecrystallized grain from Position 7 (ε ≈ 0.3) of DTC forged in the billet direction (BD)

Figure 16. Recrystallization fraction component of AD730 DTCs forged in the billet (BD) and cogging directions (CD) as function of the strain (ε = 0.3 – 2 mm/mm). Blue, yellow

and red colours correspond to recrystallized, structured and deformed grains, respectively.

Figure 17. Fractions of recrystallized, substructure and deformed grains (recrystallized fraction component) versus the effective strain for AD730 DTCs forged in the billet (BD) and cogging (CD) directions.,

Figure 18. Evolution of LAGB ($2^\circ < \theta < 10^\circ$), MAGB ($10^\circ < \theta < 15^\circ$), HAGB ($\theta > 15^\circ$), CSL and Σ3, Σ9 and Σ27 boundaries with effective strain for AD730 DTCs forged in the billet (BD) and cogging (CD) directions for recrystallized (Rex) and unrecrystallized (UnRex) regions,

Figure 19. Evolution of mean grain size in recrystallized (Rex) and unrecrystallized (UnRex) regions a) and maximum grain size b) with effective strain for AD730 DTCs forged in the billet (BD) and cogging (CD) directions.

Figure 20. Fraction evolution of Σ3 boundaries which satisfy the Brandon criterion ($v/v_m \leq 0.2$) with effective strain for AD730 DTCs forged in the billet (BD) and cogging (CD) directions.,

Figure 21. Relationship between the fraction of Σ3 which satisfy the Brandon criteria ($v/v_m \leq 0.2$) and percentage of fully recrystallized (strain-free) grains for AD730 DTCs forged in the billet (BD) and cogging (CD) directions.

10.Table captions

Table 1. Strain distribution for the 8 selected regions of hot forged AD730 DTCs

Highlights

- Large unrecrystallized grains present a fine distribution of intragranular γ’ precipitates;
- Intragranular precipitates play a key role on strain distribution and subsequent recrystallization behaviour for AD730;
- Continuous dynamic recrystallization (CDRX) promotes the gradual consumption of the large unrecrystallized grains by a new recrystallized structure.
- Undissolved secondary precipitates are playing a key role on the microstructural evolution AD730 in those position with relative low levels of deformation;
- No significant effect associated to the forging direction on the recrystallization behaviour of AD730 was found.